Experimental and Numerical Investigation of Unforced unsteadiness in a Vaneless Radial Diffuser

Giorgio Pavesi, Antoine Dazin, Giovanna Cavazzini, Guy Caignaert, Gérard Bois, Ardizzon Guido

EXPERIMENTAL AND NUMERICAL INVESTIGATION OF UNFORCED UNSTEADINESS IN A VANELESS RADIAL DIFFUSER

Giorgio Pavesi Antoine Dazin** Giovanna Cavazzini* Guy Caignaert* Gérard Bois** Guido Ardizzon**

*Department of Mechanical Engineering, University of PADOVA, Italy giorgio.pavesi@unipd.it
** Laboratoire de Mécanique de LILLE (UMR CNRS 8107), Arts et Métiers ParisTech, École antoine.dazin@ensam.lille.fr

ABSTRACT

The paper reports combined experimental and numerical investigations of unforced unsteadiness in a vaneless radial diffuser.

Experimental data were obtained within the diffuser using stereoscopic time resolved Particle Image Velocimetry (PIV) recording three velocity components in a plane (2D/3C), coupled with unsteady pressure transducers. To characterize the inception and the evolution of the unsteady phenomena, spectral analyses of the pressure signals were carried out both in frequency and time-frequency domains and the PIV results were post processed by an original averaging method.

Two partial flow rates were investigated in detail in this paper. A single unforced unsteadiness was identified for the lowest flow rate, whereas, two competitive intermittent modes were recognized for the higher mass flow.

Numerical analyses were carried out on the same pump by the commercial code CFX. All the computations were performed using the unsteady transient model and the turbulence was modelled by the Scale-Adaptive Simulation (SAS) model. Numerical pressure signals were compared with the experimental data to verify the development of the same pressure fluctuations.

INTRODUCTION

Numerous articles are available which explicitly explore the impeller diffuser interactive phenomenon by theoretical, experimental and numerical methods with the attempt to help understanding the complex unsteady flow associated with the stator rotor interaction.

Among the unsteady phenomena, the rotating stall is undoubtedly one of the most studied in the last decades. Theoretical analyses (Jansen, 1964; Senoo and Kinoshita, 1977; Fringe and Van Den Braembussche, 1985; Tsujimoto et al., 1996], as well as experimental and numerical analyses [Kinoshita and Senoo, 1985; Nishida and Kobayshi, 1988; Kobayshi and Nishida, 1990; Ferrara et al., 2002; Cellai et al., 2003; Carnevale et al., 2006; Ljevar et al, 2006; Chuang et al., 2007) were carried out to highlight the geometrical and flow parameters effects, and the flow mechanisms that can lead to its occurrence.

Several experimental and numerical analyses were also carried out on substantial flow fluctuations propagating at a low frequency, but not limited to parts of components or connected with the interaction between rotor and stator elements. Unsteady flows and pressure fluctuations developing inside centrifugal pumps and their connection with the impeller/diffuser geometries and with the operating conditions were studied by Arndt et al. (1989), Dong et al. (1997), Fatsis et al. (1997), Wuibaut et al. (2000, 2001a&b, 2002), Parrondo-Gayo et al. (2002), Guo and Okamoto (2003), Furukawa et al. (2003), Hong and Kang (2004), Akhras et al. (2004), Majidi (2005), Rodriguez et al. (2007), Dazin et al (2008), Pavesi et al. (2008), Cavazzini et al. (2009) and Feng et al. (2009).

This paper was focused on the so called "unforced unsteadiness" of the flow in a radial flow pump (Fernandez Oro et al., 2009), i.e. on the unsteady phenomena not connected with the blade passage frequency. The development of these instabilities insides turbomachines negatively affects their performance in terms of efficiency, vibrations, stability and noise emission. The object of the research was to identify the instabilities developing inside a vaneless radial diffuser. For that purpose, the experimental results obtained at partial loads by a time resolving PIV and unsteady pressure transducers were characterized by the help of a measurement techniques resolved both in time and space in order to guarantee a detailed data sampling and an in-depth analysis of the temporal and spatial evolution of the unsteady phenomena.

Linear and higher order analyses were applied to the signals to spectrally characterize the unsteady phenomena and the energy-frequency-time distributions were discussed to identify the dominant unsteadiness. Subsequently, dedicated phase-averaging technique, based on the spectral results, was developed to capture and visualize the unsteadiness evolution.

The experimental data, obtained using the 2D/3C PIV, were compared with the results of numerical analyses carried out with the help of the CFX code.

NOMENCLATURE

b	impeller or diffuser width	(m)	
c	absolute velocity	(m/s)	
cm	meridionl component of the absolute velocity	(m/3)	
$c_p=(p_4-p_3)/(0.5\rho\, c_3^2)$	pressure recovery coefficient		
f	frequency	(Hz)	
h	pump head	(m)	
p	pressure	(Pa)	
Q	volume flow rate	(m^3/s)	
r	radial position	(m)	
R	radius	(m)	
$Re= u_2 R_2/\nu$	Reynolds number		
u	peripheral velocity	(m/s)	
Z	number of impeller blades		
$\psi=gh/u_2^2$	head coefficient		
ρ	density	(kg/m^3)	
ν	kinematic viscosity	(m^2/s)	
ω	angular rotation velocity	(rad/s)	
$\omega_s=\omega\, Q_n^{0.5}/(\Delta p/\rho)^{0.75}$	specific speed		

Subscripts

1	impeller inlet	d	design
2	impeller outlet	r	radial component
3	diffuser inlet	u	tangential component
4	diffuser outlet		

EXPERIMENTAL SET-UP

The experimental analyses were carried out on a centrifugal impeller coupled with a vaneless diffuser with no volute downstream the diffuser to guarantee the flow field axial symmetry. The main geometry characteristics of the tested pump, as well as the flow rate at the design points were reported in table 1. Figure 1 show the pump characteristics and the pressure recovery coefficient of the diffuser.

Table 1: Pump characteristics

Impeller outlet radius R_2	256.6 mm
Impeller inlet tip radius R_1	141.1 mm
Number of blades Z	7 -
Outlet width b_2	38.5 mm
Design flow rate at 1200 rpm Q_d	0.236 m^3/s
Specific speed ω_s	0.577
Design head h	51.0 m
Reynolds number $Re = u_2 R_2/\nu$	$5.52\cdot10^5$ -
Diffuser inlet radius R_3	257.1 mm
Diffuser outlet radius R_4	390 mm
Diffuser width b_3	40 mm

The tests were made in an air test rig schematized in figure 2, developed for studying the rotor-stator interaction phenomena. The test rig is properly built for the application of optical analysis methods and in particular of the Particle Image Velocimetry (PIV) technique: the walls of the dif-

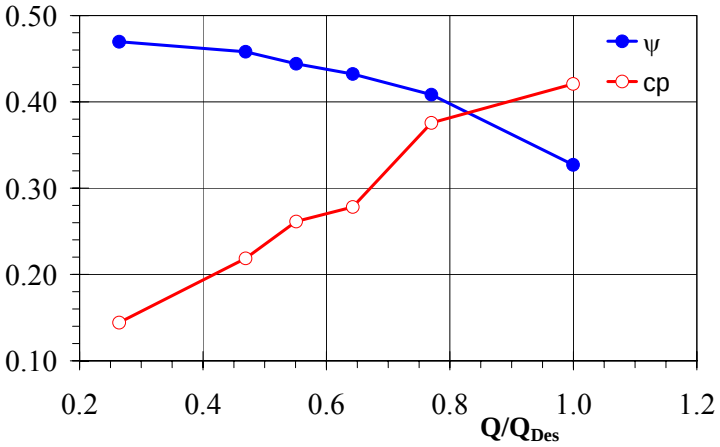

Figure 1 Head coefficient and pressure recovery factor versus percentage flow rate.

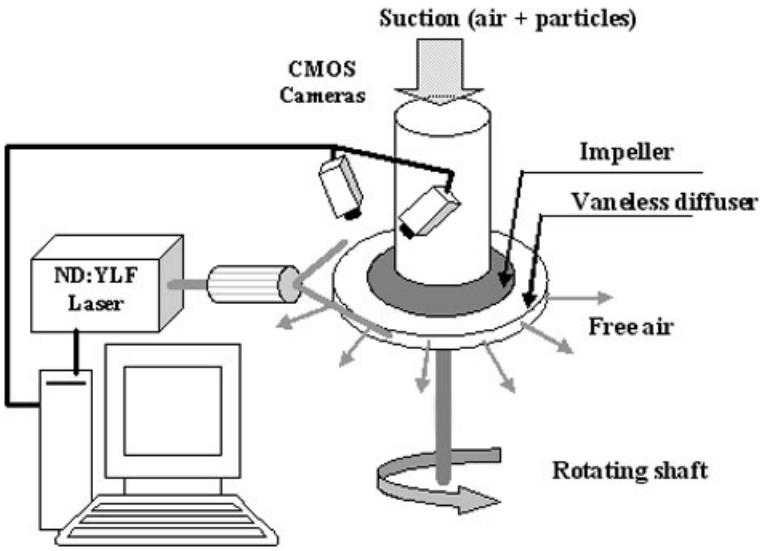

Figure 2 Experimental set-up

fuser are transparent and the lack of volute downstream the diffuser allows large optical access for the laser sheet and the cameras. It was already used in previous studies carried out on the same impeller coupled with a short vaneless diffuser [Wuibaut et al., 2001 a&b, 2002] and two different types of vaned diffusers [Cavazzini et al., 2009].

In the present study, to favour the complete development and stabilization of the unsteady interaction phenomena at the impeller discharge, a vaneless diffuser having an outlet radius larger than the previous one was coupled with the impeller.

The flow field inside the diffuser was studied by a 2D/3C High Speed PIV having a ND: YLF Laser with an energy pulse of 20 mJ and a pulse duration of 90 ns. Both laser cavities were characterized by a sampling frequency of 980 Hz with a time delay between their pulses fixed equal to 110 or 130 μs depending on the flow rate. A light sheet approximately 90 mm wide with a thickness of 1.5 mm was obtained at three heights in the hub to shroud direction (b/b_3 = 0.25, 0.5 and 0.75) using conventional optical components (2 spherical and a cylindrical lenses).

Two identical CMOS cameras (Phantom V9), equipped with 50 mm lenses, recorded PIV snapshots (1680 x 930 pixel^2). They were located at a distance of 480 mm from the measurement regions. The angle between the object plane and the image plane was about 45°. As regards the seeding, incense smoke particles having a size of less than 1 μm were used.

The image treatment was performed by software developed by the Laboratoire de Mécanique de Lille. The cross-correlation technique was applied to the image pairs with a correlation window size of 32*32 pixels^2 and an overlapping of 50%, obtaining flow fields of 80*120 mm^2 and 81*125 velocity vectors. A three points Gaussian model fit the correlation peaks. The mean image particle size, estimated by image treatment, was 1.7 pixels and about 17 particles were identified in each correlation window of 32 x 32 pxl^2. Taking into account the measurement uncertainty, determined using a quiescent flow, as well as the main parameters having an influence on PIV accuracy (particle size and density, loss of particles, velocity gradients) (Foucaut et al, 2004), the uncertainty in the velocity measurements was about 5%. In particular, the following uncertainties were determined: 0.05 pxl for peak-locking, 0.01 pxl due to the particle loss linked with the velocity component normal to the laser sheet and less than 0.15 pxl due to velocity gradients. The accuracy of the reconstruction algorithm was estimated to be of about 0.1 pxl.

Each PIV measurement campaign was carried out for a time period of 1.6 second, corresponding to 32 impeller revolutions at a rotation speed of 1200 rpm. Since the temporal resolution of the

acquisition was of 980 velocity maps per second, the time period of 1.6 second allowed obtaining 1568 consecutives velocity maps, corresponding to about 49 velocity maps per impeller revolution

Four Brüel & Kjaer condenser microphones (Type 4135) were used for the unsteady pressure measurements, two of them were flush mounted on the shroud side of the diffuser wall and were located at the same radial position (r/r_3=1.05) but at different angular position ($\Delta\theta$=75°). The other two microphones were flush mounted on the suction pipe of the pump at a distance of 150 mm from the impeller inlet. The data were acquired by a LMS Difa-Scadas system with a sampling frequency of 2048 Hz. The measurement uncertainty for these measurements was less than 1 %. To synchronize the unsteady pressure measurements with the velocity maps, a signal was sent by the PIV system to the LMS Difa-Scadas acquisition system.

The operating conditions were regulated by normalized diaphragms (norm NF X 10-102). Experimental measurements were acquired for the design flow rate Q_d and at 5 partial flow rates (0.26 Q_d, 0.45 Q_d, 0.56 Q_d, 0.66 Q_d and 0.75 Q_d) with an impeller rotation speed of 1200 rpm.

The results here presented refer to the two lowest analysed flow rates (0.26 and 0.45 Q_d) and focus to PIV measurements obtained at mid span.

NUMERICAL PROCEDURE

Computations were performed by using the commercial code CFX 12.0. The Scale-Adaptive Simulation (SAS SST) turbulence model, with the transition to laminar based on two transport equations, one for the intermittency and one for the transition onset criteria in terms of momentum thickness Reynolds number, was adopted for the pump simulations

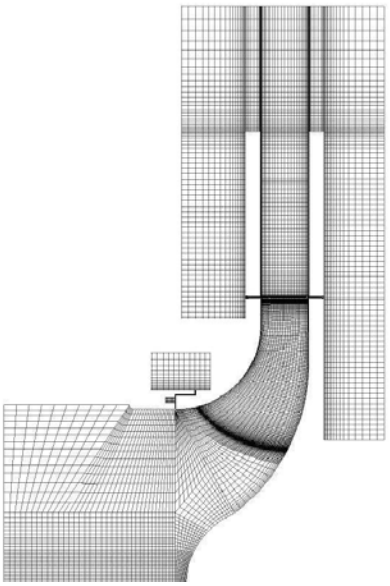

Figure 3 Coarse mesh of part of the inflow, the impeller and the outlet

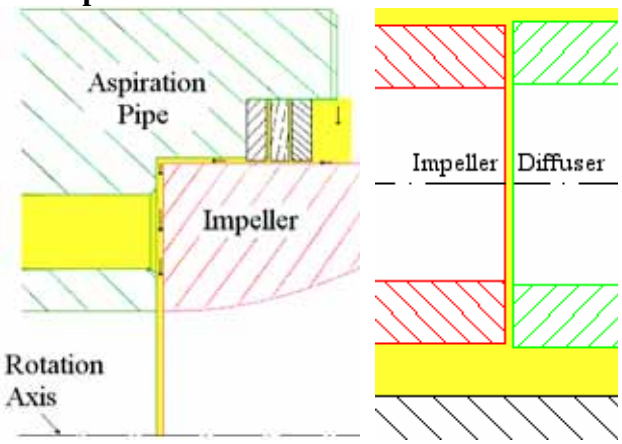

Figure 4 Seal system at the impeller inlet (left) and outlet (right).

The SAS model was utilized in order to take advantage of its ability to result a LES-like (Large Eddy Simulation) behaviour in unsteady regions of the flow field and, at the same time, to provide standard RANS (Reynolds Averaged Navier Stokes) capabilities in stable flow regions

An unsteady model was used for all the computations. For the interface between stator/rotor blocks the standard transient sliding interface approach was chosen. For the discretization in time a second order dual time stepping scheme was adopted. The time step for the explicit scheme was chosen according to a rotation of the runner, of about one degree resulting in a Courant Number of about CFL=1.5. The maximum number of iterations for each time step is set to 5, in order to give mass residues of 10^{-6}, momentum residues of10^{-4}, turbulence kinetic energy and energy dissipation of 10^{-4}.

A J-type grid was used for the impeller, whereas an H-type grid was adopted for the diffuser. The leakage from the labyrinth seal was also considered (figs 3 and 4) and several H-blocks were built to describe the cavities. The grid was globally of $9.2 \cdot 10^6$ points, with y+ values below 10 in the entire computational region.

As regards the boundary conditions, mass flow rates obtained from the experimental data

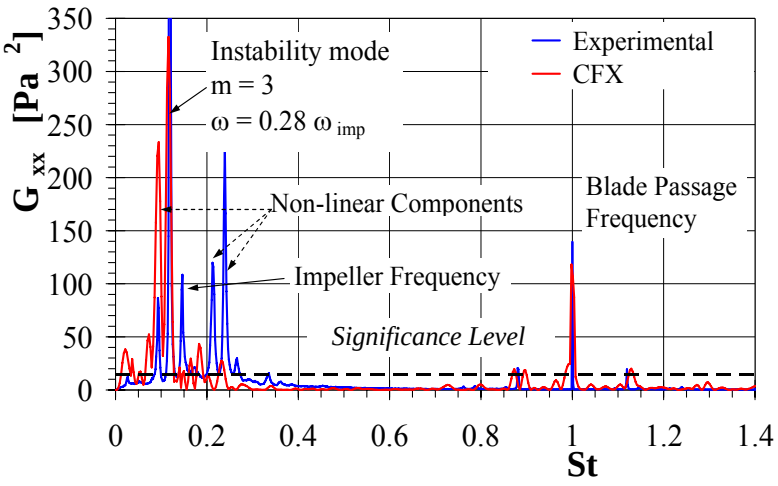

Figure 4 Cross-power spectra of the microphones located in the diffuser at $Q/Q_d = 0.26$.

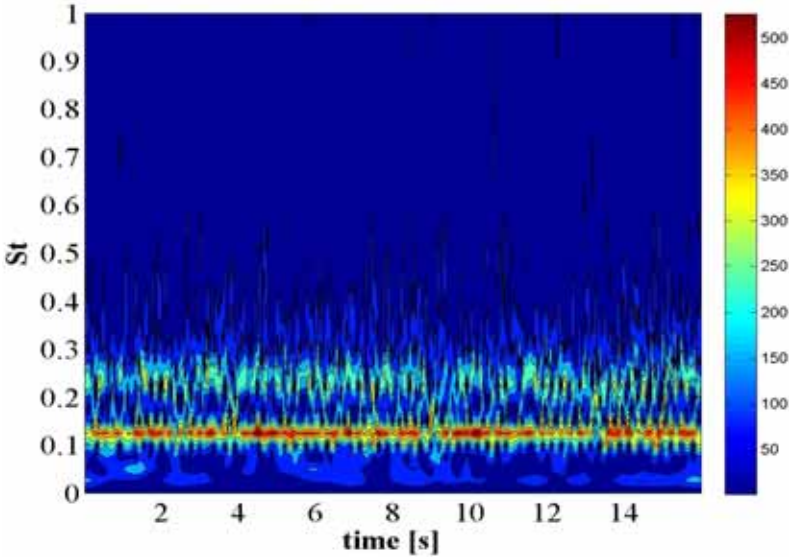

Figure 5 Wavelet analysis at $Q/Q_d = 0.26$.

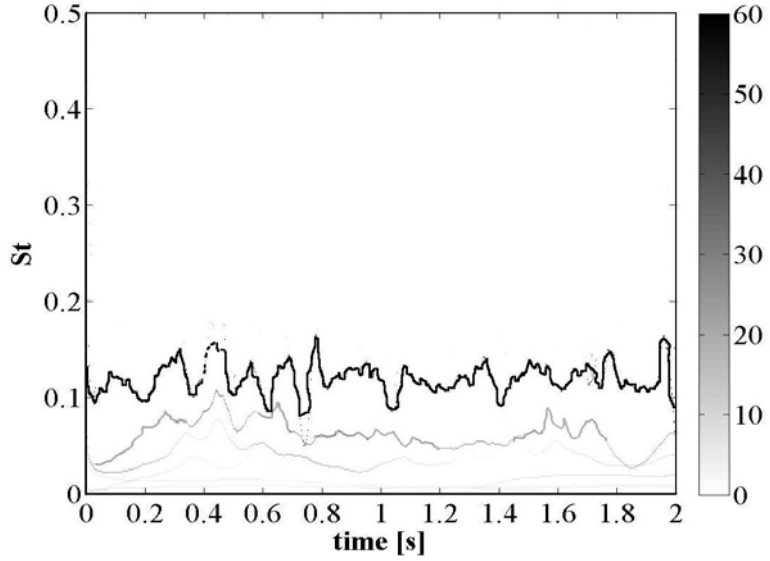

Figure 6 Hilbert spectrum at $Q/Q_d = 0.26$.

were prescribed at the inlet boundary and at the labyrinth close to the impeller inlet with stochastic fluctuations of the velocities with 5 % free-stream turbulence intensity. At the impeller outlet the leakage mass flow rate was controlled by the known pressure in the large plenums upstream the labyrinth.

The surfaces were supposed as adiabatic walls with a no-slip condition. As for the exit boundary conditions, the experimental pressure level was prescribed as an average pressure at the diffuser outlet.

RESULTS

For the lower flow rate (0.26 Q_d), the cross-power spectrum of the pressure transducers located in the diffuser was dominated by a subtonal frequency (St =0.12) (Fig. 4).

The analysis of the phase and amplitude of the cross-power spectra of the pressure signals allowed for the identification of the origin of this pressure pulsation. This was due to three cells, rotating with an angular velocity equal to 28 percent of the impeller one. The wavelet analysis, computed using a Morlet mother wavelet showed that the peak associated with the rotating pressure pulsation dominated the spectrum all over the time (Fig 4). Moreover, to eliminate the spurious harmonics resulting from imposing a linear structure on the nonlinear system and to obtain more accurate identifications of the unsteady and non-linear structures embedded in the time-series, the Hilbert-Huang transform developed by Huang et al. (1996,1998,1999) was applied.

The transform was subdivided in two steps. By the empirical mode decomposition the signal was decomposed into a finite number of "intrinsic mode functions", next to the Hilbert transform was applied to these functions to determine the instantaneous frequency of each of these components.

The final result was the energy-frequency-time distribution shown in figure 6. The result

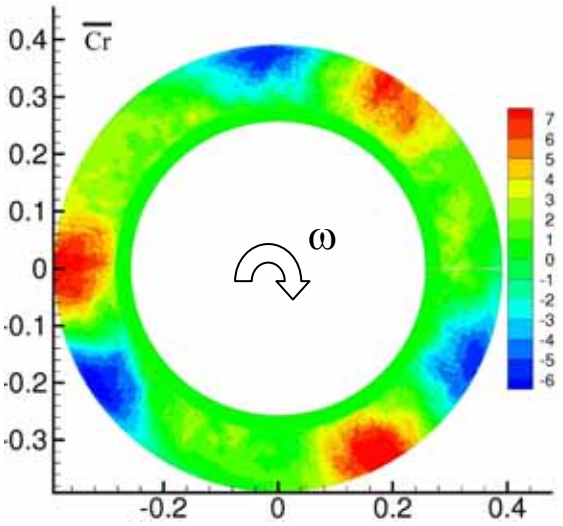

Figure 7 Results of the averaging of 1581 consecutives velocity maps in a frame rotating with the instability

highlights the mode that was marked by constant high energy and it dominated the diffuser flow field.

To capture and visualize the unsteady flow field associated with the instability, the averaging method of the velocity fields, based on the determined instability precession velocity (Cavazzini et al 2008, Dazin et al 2009), was adopted.

Each velocity map obtained by the PIV analysis was considered like a tessera of a mosaic whose position in the diffuser was linked to the instability evolution. To achieve this, it was assumed the frame rotates with the instability. Consistently the map was rotated of an angle equal to the instability velocity multiplied by the sampling period of the PIV measurements. In the overlapping zones between two or more maps the velocity values were averaged.

The resulting averaged radial and tangential velocity flow fields are presented in fig. 7. Three cells with similar topologies are clearly identifiable. They are composed of two cores respectively of inward and outward radial velocities, located near the diffuser outlet. Between these cores it is possible to identify a zone of negative tangential velocity.

To investigate the possible origin of this instability, a numerical analysis was carried out on the same configuration and its capability to capture pressure unsteadiness was verified.

The pressure signals were acquired for about 23 impeller revolutions, corresponding to one sample of about 1.2s after the simulation convergence obtained next to 20 impeller revolutions. The sampling frequency of the numerical pressure signal was 7142 Hz and the resolution of the numerical spectrum was about 1.3 Hz.

The agreement between numerical and experimental spectral results was quite good, as it can be seen in fig. 4 reporting the power spectra of the numerical and experimental pressure signals acquired in the diffuser. Numerical and experimental peaks have similar amplitude but the numerical analysis does not appear to be able to capture the non linear components that dominate the low frequency signal.

The significance level of the numerical power spectrum at 99% is equal to 12 [Pa^2] and consistently quite all the peaks highlighted by the numerical analysis have significance.

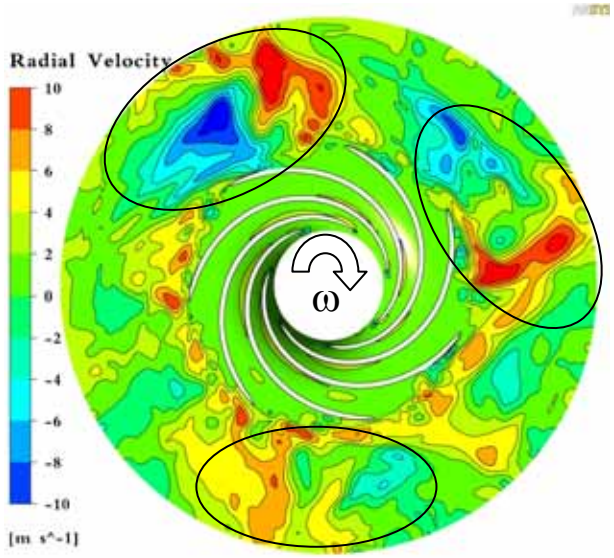

Figure 8 Radial velocity component inside the diffuser and in the free field at Q/Q_d=0.26.

Fig. 8 shows radial velocity component maps obtained by the numerical analysis at mid diffuser height. In agreement with the experimental observations three rotating instabilities, composed by a core of outward radial velocity followed by a zone of inward radial velocity, are quite well identifiable. The cores changes appeared to be associated with the jets coming out from the impeller discharge. Fig. 9 reports the time evolution of the flow field in the diffuser cross section in correspondence of one core and the contemporaneous evolution of the flow field far from the core. The incoming jet forced the blockage of the vortexes, which were pushed towards the diffuser outlet and confined near the walls (Fig. 10a, t_1-t_4). The jet action appears to reinforce the instability supplying

the energy to enlarge and/or to preserve its action.

When the forcing action of the jet vanished, the vortices progressively reoccupied the whole diffuser width, starting again the blockage action till a new jet arrived.

At 45% of the design flow rate, two low frequency peaks were identified in the cross power spectrum of the pressure transducers (Fig. 10). The first mode, which dominated the spectrum, corresponded to an instability composed by two cells rotating at $\omega = 0.28*\omega_{imp}$. The second corresponded to an instability composed by three cells rotating at $\omega = 0.28*\omega_{imp}$.

The time frequency analysis (Figs 11 and 13) demonstrates that these two competitive modes were present intermittently and never existed at the same time.

Consistently the Hilbert spectrum (Fig. 12) pointed out the two modes were characterized by variable energy level. The two instabilities appear to be strongly energy-consumptive and competitive. Each instability tends to absorb quite all the energy, to stabilize its structure and to disrupt the other unsteadiness. For the flow rate 0.45 Q_d, the instabilities did not succeed in catching up with stability and a dominance to prevent the appearance of unsteadiness. Consistently, the two instabilities were formed alternatively into the diffuser.

The agreement between numerical and experimental spectral results was confirmed also with the flow rate 0.45 Q_d, as it can be seen in fig. 10. Nevertheless, the pressure instability identified by

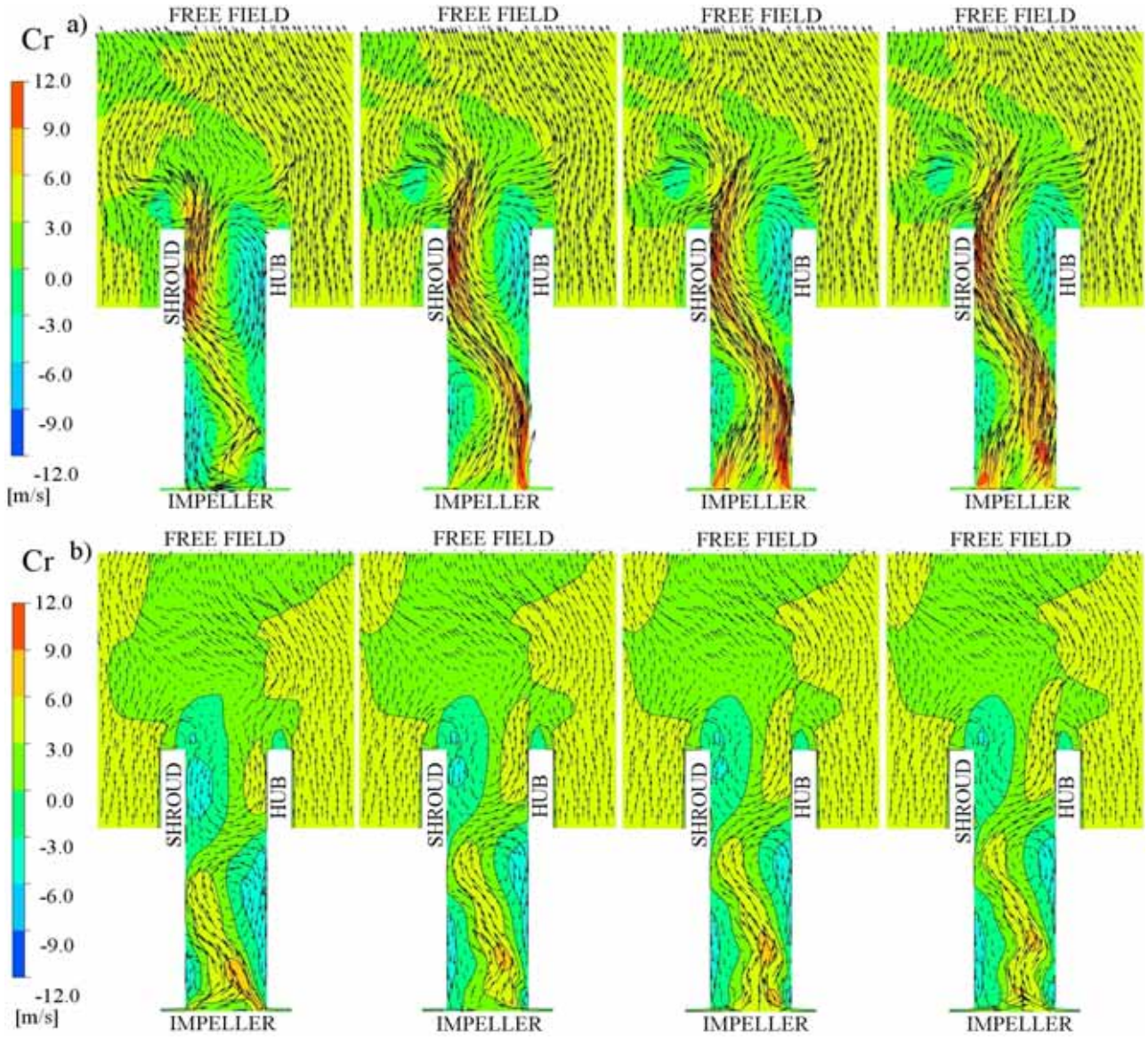

Figure 9: Evolution of the flow field inside the diffuser at Q/Q_d = 0.26. Meridional sections built respectively in the presence (a) or not (b) of one pattern.

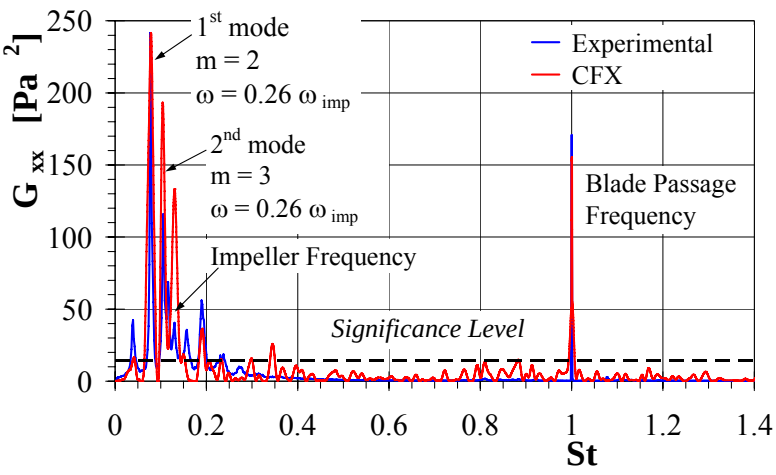

Figure 10 Cross-power spectrum of the microphones located in the diffuser at Q/Q_d = 0.45.

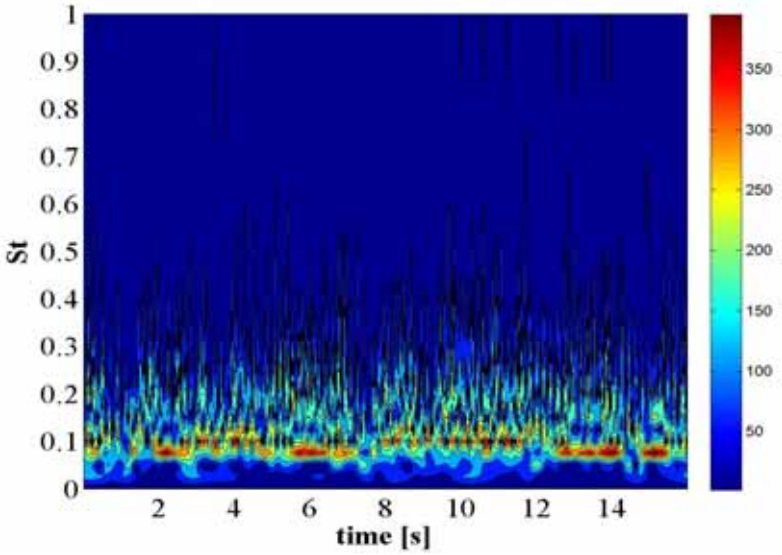

Figure 11 Wavelet analysis - Q/Q_d = 0.45.

the numerical analysis presented an evolution in time a little bit different of the experimental one, as it can be seen by comparison of the wavelets spectra reported in fig. 13. The numerical analysis appears to be dominated by the second mode fluctuating instability contrary to the experimental results.

The results of the time frequency analyses were used to determine time periods during which only one mode is dominant. The PIV averaging procedure was then applied to only these time periods. The results of this averaging on a time period when the first mode and the second mode are present are presented in fig. 14.

For the first mode a time period of about 0.4 s is identified at the beginning of the simultaneous pressure and PIV acquisitions. Consistent with Fourier spectra analysis, the PIV averaged velocity map (fig. 14a) obtained on this time period presents two instability cells diametrically located, similar to those obtained at the lowest flow rate.

For the second mode, the longer time period identified was of only about 0.1 s. The averaged velocity procedure applied on this time period gives the velocity map plotted on fig 14b. For this mode, the expected number of cells was three, whereas, the averaged velocity map presents only two clear cells (surrounded by a solid line). The third cell of this mode is hardly visible (inside the dashed lines), most probably due to the period being too short to perform the PIV averaging procedure.

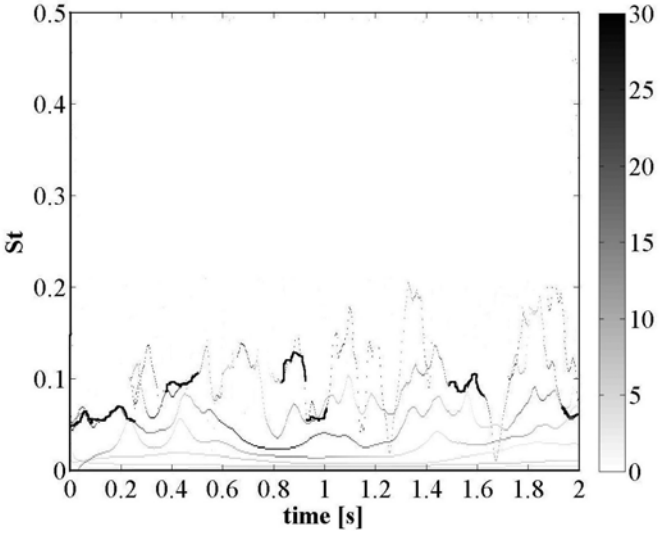

Figure 12 Hilbert spectrum at Q/Q_d = 0.45.

The radial velocity component maps obtained by the numerical analysis at mid diffuser height is shown in figure 15. Until in the time interval considered, the second mode prevailed the numerical analysis only three rotating instabilities were identifiable. Two of them (surrounded by a solid line) were clearly identifiable. The third cell (inside the dashed lines) was progressively growing up and defining its action in the analyzed time period. Differently from the lower flow rate at Q/Q_d=0.45 the jet coming out the impeller showed a more progressive and less aggressive action that endeavours to interest all the diffuser channel (fig. 16).

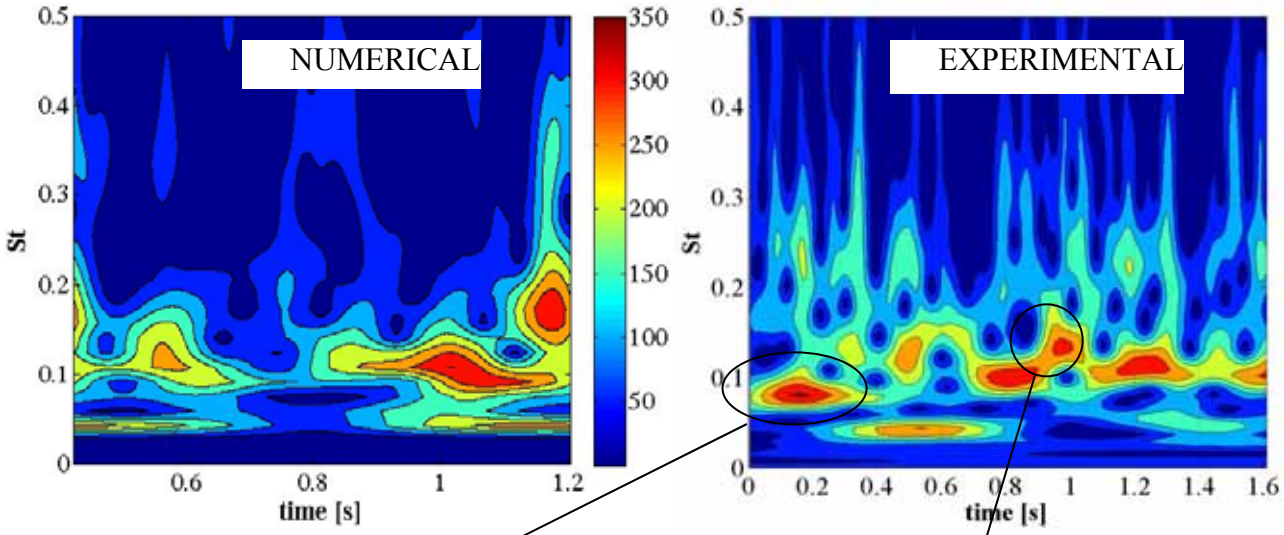

Figure 13 Detail wavelet analysis at $Q/Q_d = 0.45$.

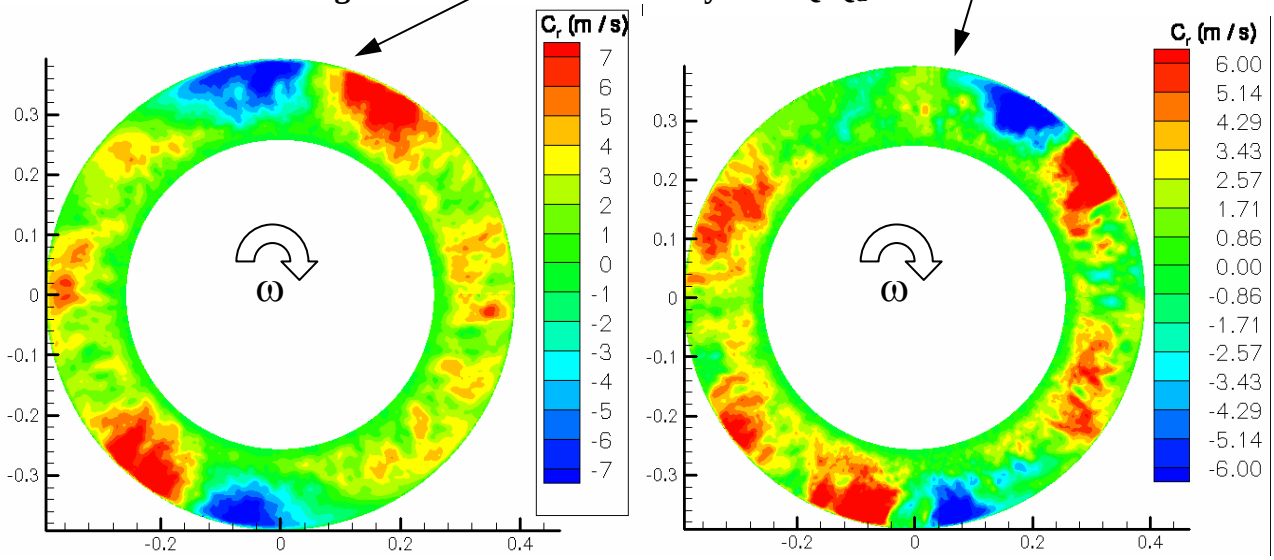

Figure 14 PIV averaging procedure results for the two modes identified at $Q/Q_d = 0.45$

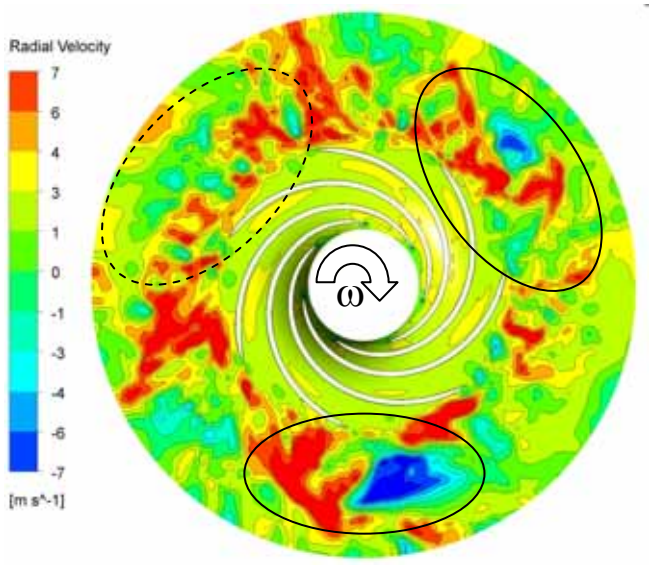

Figure 15 Radial velocity component inside the diffuser and in the free field at $Q/Q_d = 0.45$.

CONCLUSIONS

A vaneless diffuser of a radial flow pump was experimentally and numerically investigated at two partial flow rates. The experiments were performed with the high repetition rate PIV coupled with unsteady pressure transducers placed flush the shroud wall of the diffuser. The analysis of the pressure fluctuations and of numerical simulations has shown that rotating instability develops for the two flow rates. A PIV averaging technique was used to visualize the rotating cells composing the instability. Each cell was composed of two cores of respectively inward and outward radial velocities, located near the diffuser outlet. Between these cores it was possible to identify a zone of negative tangential velocity and a zone of slightly positive axial velocity component. But whereas only one instability mode (3 cells rotating at 0.28 ω_{imp}) developed at the lower flow rate (0. 26 Q_d), two different modes (with 2 or 3 cells) were

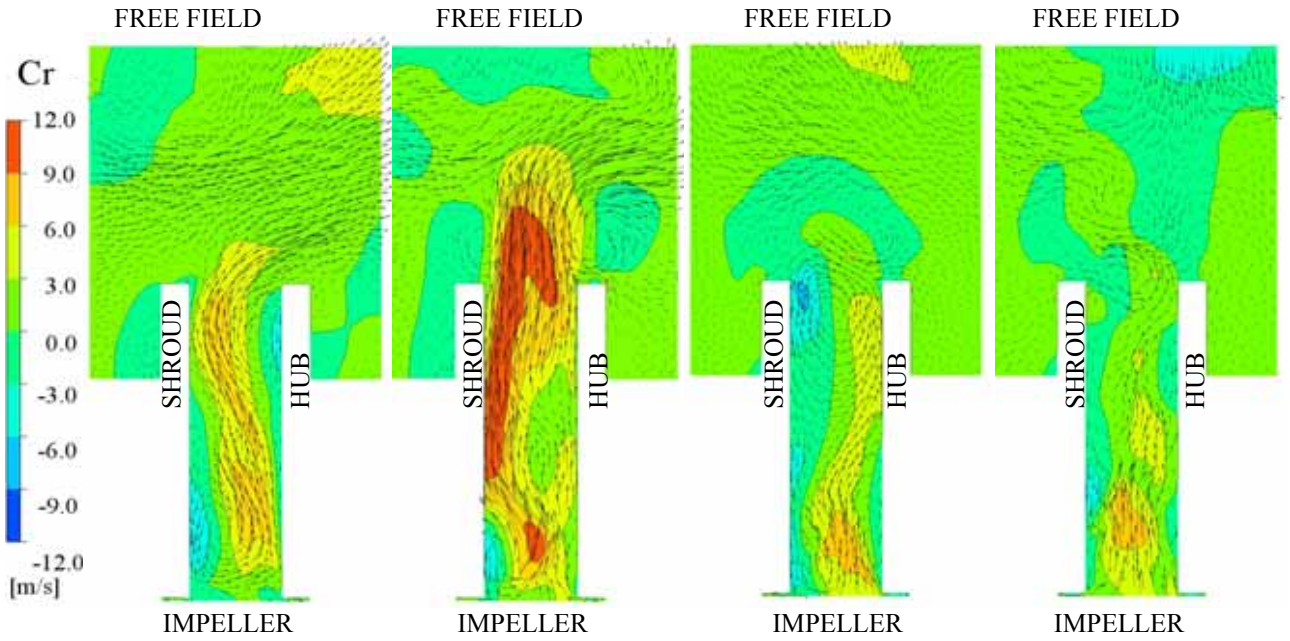

Figure 16 Evolution of the flow field inside the diffuser at Q/Q_d = 0.45. Meridional sections built respectively in the presence (a-b) or not (c-d) of one pattern.

intermittently active at 0.45 Q_d.

The instabilities appear to be strongly energy-consumptive. Each instability tends to absorb quite all the energy, to stabilize its structure and to disrupt the other unsteadiness.

The impeller trigger appears to determine an angle fluctuation perturbing the diffuser flow field and favouring the unstable development of the modes.

However, more in-depth analyses are necessary to demonstrate the combined effect of the impeller trigger and of the diffuser unstable characteristics.

ACKNOWLEDGMENTS

The authors wish to thank the Nord Pas de Calais Region and the International Campus on Safety and Intermodality in Transportation (CISIT) for their support to this research project.

REFERENCES

AKHRAS A., EL HAJEM M., CHAMPAGNE J.-Y., MOREL R. (2004), The Flow Rate Influence on the Interaction of a Radial Pump Impeller and the Diffuser. International Journal of Rotating Machinery, vol. 10, no. 4, pp. 309-317

ARNDT N., ACOSTA A. J. , BRENNEN C. E., CAUGHEY T. K. (1989), Rotor-stator interaction in a diffuser pump, Journal of Turbomachinery, vol. 111, no. 3, pp. 213–221.

CARNEVALE E.A., FERRARA G., FERRARI L., BALDASSARRE L. (2006), Experimental Investigation and characterization of the rotating stall in a high pressure centrifugal compressor. Part VI: Reduction of three impeller results. Proceedings of ASME, International Gas Turbine Institute, Turbo Expo 2006 - Power for Land, Sea and Air, vol. 6B, pp. 1105-1112, Barcelona, Spain, May 6-May 11, 2006.

CAVAZZINI G., DAZIN A., PAVESI G., DUPONT P., CAIGNAERT G., BOIS G., ARDIZZON G. (2008) *Rotating instability in a radial vaneless diffuser.* 24th Symposium on Hydraulic Machinery and Systems. IAHR. Foz de Iguazu. Brazil. 26 – 30 Oct 2008.

CAVAZZINI G., PAVESI G., ARDIZZON G., DUPONT P., COUDERT S., CAIGNAERT G., BOIS G. (2009), Analysis of the Rotor-Stator Interaction in a Radial Flow Pump. La Houille Blanche, Revue Internationale de l'eau, n. 5/2009, pp. 141-151.

CELLAI A., FERRARA G., FERRARI L., MEGNONI C.P., BALDASSARRE L. (2003), Experimental Investigation and characterization of the rotating stall in a high pressure centrifugal compressor. Part III: Influence of diffuser geometry on stall inception and performance (2nd impel-

ler tested). Proceedings of ASME, International Gas Turbine Institute, Turbo Expo, IGTI, vol. 6B, pp. 711-719, Atlanta, GA, United States, June 16 – June 19, 2003.

CHUANG G., CHUANGANG G., TONG W., BO Y. (2007), Analysis of Geometries' Effects on Rotating Stall in Vaneless Diffuser with Wavelet Neural Networks. International Journal of Rotating Machinery, vol. 2007, Article ID 76476, 10 pages, doi: 10.1155/2007/76476

DAZIN A., COUDERT S., DUPONT P., CAIGNAERT G., BOIS G. (2008), Rotating Instability in the Vaneless Diffuser of a Radial Flow Pump. Journal of Thermal Science. Dec 2008, 17(4), 368-374.

DAZIN A., COUTIER-DELGOSHA O., DUPONT P., COUDERT S., CAIGNAERT G., BOIS G. (2008) *Rotating Stall in the Vaneless Diffuser of a Radial Flow Pump*., J Therm Sci., 17(4), 368-374.

DAZIN A., CAVAZZINI G., PAVESI G., DUPONT P., CAIGNAERT G., BOIS G., ARDIZZON G. (2009) *Rotating instability in a radial vaneless diffuser. Part 1 : High speed stereoscopic PIV measurements.* 8th European Conference on Turbomachinery, Graz, March 2009

DONG R., CHU S., KATZ J. (1997), Effect of Modification to Tongue and Impeller Geometry on Unsteady Flow, Pressure Fluctuations, and Noise in a Centrifugal Pump. Transaction of ASME, Journal of Turbomachinery, vol. 119, no. 3, pp. 506-515

DOU H.-S., MIZUKI S. (1998), Analysis of the flow in vaneless diffusers with large width-to-radius ratios. Journal of Turbomachinery, vol. 120, no. 1, pp. 193-201

FATSIS A., PIERRET S., VAN DEN BRAEMBUSSCHE R. (1997), Three-dimensional Unsteady Flow and Forces in Centrifugal Impellers with Circumferential Distortion of the Outlet Static Pressure. Transaction of ASME, Journal of Turbomachinery, vol. 119, no. 1, pp. 94-102

FENG J., BENRA F.-K., DOHMEN H.J. (2009), Unsteady Flow Visualization at Part Load Conditions of a Radial Diffuser Pump: by PIV and CFD. Journal of Visualization, vol. 12, no. 1, pp. 65-72.

FERNANDEZ ORO J.M., BLANCO MARIGORTA E., ARGÜELLES DIAZ K.M. (2009), Forced and unforced unsteadiness in an axial turbomachine. Experimental Thermal and Fluid Science, vol. 33, no. 3, pp. 449-459.

FERRARA G., FERRARI L., MEGNONI C.P., DE LUCIA M., BALDASSARRE L. (2002), Experimental Investigation and characterization of the rotating stall in a high pressure centrifugal compressor. Part I: influence of diffuser geometry on stall inception. Proceedings of ASME, International Gas Turbine Institute, Turbo Expo, IGTI, vol. 5A, pp. 613-620, Amsterdam, The Netherlands, June 3 - June 6, 2002.

FOUCAUT J.M., MILIAT B., PERENNE N., STANISLAS M., (2004), *Characterisation of different PIV algortihms using the EUROPIV synthetic image generator and real images from a turbulent boundary layer.* Proceeding of the EUROPIV 2 workshop on Particle Image Velocimetry. Springer, Berlin Heidelberg New York, pp 163-186.

FRINGE P., VAN DEN BRAEMBUSSCHE R. (1985), A theoretical model for rotating stall in the vaneless diffuser of a centrifugal compressor. ASME Journal of Engineering for Gas Turbines and Power, vol. 107, no. 2, pp. 507-513

FURUKAWA A., TAKAHARA H., NAKAGAWA T., ONO Y. (2003), Pressure fluctuation in a vaned diffuser downstream from a centrifugal pump impeller, International Journal of Rotating Machinery, vol. 9, no. 4, pp. 285–292.

GUO S., OKAMOTO H. (2003), An experimental study on the fluid forces induced by rotor-stator interaction in a centrifugal pump. International Journal of Rotating Machinery, vol. 9, no. 2, pp. 135-144.

HONG S.-S., KANG S.-H. (2004), Flow at the Centrifugal Pump Impeller Exit with the Circumferential Distortion of the Outlet Static Pressure. Transaction of ASME, Journal of Fluids Engineering, vol. 126, no. 1, pp. 81-86.

Huang, N. E., S. R. Long, and Z. Shen, 1996: The mechanism for frequency downshift in nonlinear wave evolution. Adv. Appl. Mech., **32**, 59–111.

Huang, N. E., Z. Shen, S. R. Long, M. C. Wu, H. H. Shih, Q. Zheng, N.-C. Yen, C. C. Tung, and H. H. Liu, 1998: The empirical mode decomposition and the Hilbert spectrum for nonlinear and non-stationary time series analysis. Proc.R. Soc. London, Ser. A, **454**, 903–995.

Huang, N. E., Z. Shen, and S. R. Long, 1999: A new view of water waves – The Hilbert spectrum. Annu. Rev. Fluid Mech., **31**, 417–457.

KINOSHITA Y., SENOO Y. (1985), Rotating Stall induced in vaneless diffusers of very low specific speed centrifugal blowers. Journal of Engineering for Gas Turbines and Power, vol. 107, no. 2, pp. 514-521.

KOBAYSHI H., NISHIDA H. (1990), A study on the rotating stall of centrifugal compressor (2nd report, effect of vaneless diffuser inlet shape on rotating stall). Transactions of JSME, Series B, vol. 56, no. 529, pp. 98-103.

JANSEN W. (1964), Rotating stall in a radial vaneless diffuser. Journal of Basic Engineering, vol. 86, pp. 750-758.

LJEVAR S., DE LANGE H.C., VAN STEENHOVEN A.A. (2006), Two-dimensional Rotating Stall Analysis in a Wide Vaneless Diffuser. International Journal of Rotating Machinery, vol. 2006, Article ID 56420, pp. 1-11, DOI, 10.115/IJRM/2006/56420

MAJIDI K. (2005), Numerical Study of Unsteady Flow in a Centrifugal Pump. Transactions of ASME, Journal of Turbomachinery, vol. 127, no. 2, pp. 363-371.

NISHIDA H., KOBAYSHI H. (1988), A study on the rotating stall of centrifugal compressor (1st report, effect of vaneless diffuser width on rotating stall). Transactions of JSME, Series B, vol. 54, no. 499, pp. 584-594.

PARRONDO-GAYO J.L., GONZALEZ-PEREZ J., FERNANDEZ-FRANCOS J. (2002), The Effect of the Operating Point on the Pressure Fluctuations at the Blade Passage Frequency in the Volute of a Centrifugal Pump. Transactions of ASME, Journal of Fluids Engineering, vol. 124, no. 3, pp. 784-790

PAVESI G., CAVAZZINI G., ARDIZZON G. (2008), Time-frequency Characterization of the Unsteady Phenomena in a Centrifugal Pump. International Journal of Heat and Fluid Flow, vol. 29, no. 5, pp. 1527-1540.

RODRIGUEZ C.G., EGUSQUIZA E., SANTOS I.F. (2007), Frequencies in the Vibration Induced by the Rotor Stator Interaction in a Centrifugal Pump Turbine. Transactions of ASME, Journal of Fluids Engineering, vol. 129, no. 11, pp. 1428-1435.

SENOO Y., KINOSHITA Y. (1977), Influence of inlet flow conditions and geometries of centrifugal vaneless diffusers on critical flow angle for reverse flow. Journal of Fluid Mechanics, vol. 99, no. 1, pp. 98-103

TSUJIMOTO Y., YOSHIDA Y., MORI Y. (1996), Study of vaneless diffuser rotating stall based on two dimensional inviscid flow analysis. ASME Journal of Fluids Engineering, vol. 118, pp. 123-127.

WUIBAUT G., DUPONT P., BOIS G., CAIGNAERT G., STANISLAS M. (2001), Analysis of flow velocities within the impeller and the vaneless diffuser of a radial flow pump. ImechE Journal of Power and Energy, part A, vol. 215, pp. 801-808.

WUIBAUT G., BOIS G., DUPONT P., CAIGNAERT G., STANISLAS M. (2002), PIV measurements in the impeller and the vaneless diffuser of a radial flow pump in design and off-design operating conditions. Journal of Fluids Engineering, vol. 124, no. 3, pp. 791–797.

WUIBAUT G., BOIS G., DUPONT P. and CAIGNAERT G. (2002b). *Rotor stator interactions in a vaned diffuser of a radial flow pump for different flow rates using PIV measurement technique*. 9th International Symposium on Transport Phenomena and Dynamics of Rotating Machinery, ISROMAC 9, 10 -14 February 2002, Hawaii, USA

WUIBAUT G., BOIS G., CAIGNAERT G., DUPONT P. and STANISLAS M. (2002c). *Experimental analysis of interactions between the impeller and the vaned diffuser of a radial flow pump*. XXI IAHR Symposium, September 9-12th 2002, Ecole Polytechnique Fédérale de Lausanne, Switzerland, pp. 825-836.